Journal of Applied Physics

Sorption-induced static mode nanomechanical sensing with viscoelastic receptor layers for multistep injection-purge cycles

Cite as: J. Appl. Phys. **129**, 124503 (2021); https://doi.org/10.1063/5.0039045
Submitted: 29 November 2020 . Accepted: 05 March 2021 . Published Online: 25 March 2021

Kosuke Minami, Kota Shiba, and Genki Yoshikawa

Journal of Applied Physics ARTICLE scitation.org/journal/jap

Sorption-induced static mode nanomechanical sensing with viscoelastic receptor layers for multistep injection-purge cycles

Cite as: J. Appl. Phys. **129**, 124503 (2021); doi: 10.1063/5.0039045
Submitted: 29 November 2020 · Accepted: 5 March 2021 ·
Published Online: 25 March 2021

Kosuke Minami,[1,2,a)] Kota Shiba,[2,3] and Genki Yoshikawa[2,4]

AFFILIATIONS

[1]International Center for Young Scientists (ICYS), National Institute for Materials Science (NIMS), 1-1 Namiki, Tsukuba, Ibaraki 305-0044, Japan
[2]Center for Functional Sensor & Actuator (CFSN), Research Center for Functional Materials, National Institute for Materials Science (NIMS), 1-1 Namiki, Tsukuba, Ibaraki 305-0044, Japan
[3]John A. Paulson School of Engineering and Applied Sciences, Harvard University, 9 Oxford Street, Cambridge, Massachusetts 02138, USA
[4]Materials Science and Engineering, Graduate School of Pure and Applied Science, University of Tsukuba, 1-1-1 Tennodai, Tsukuba, Ibaraki 305-8571, Japan

[a)]**Author to whom correspondence should be addressed:** MINAMI.Kosuke@nims.go.jp

ABSTRACT

Nanomechanical sensors and their arrays have been attracting significant attention for detecting, distinguishing, and identifying target analytes. In the static mode operation, sensing signals are obtained by a concentration-dependent sorption-induced mechanical strain/stress. The analytical models for the static mode nanomechanical sensing with viscoelastic receptor layers have been proposed, while they are not formulated for practical conditions, such as multistep injection-purge cycles. Here, we derive an analytical model of viscoelastic material-based nanomechanical sensing by extending the theoretical model via solving differential equations with recurrence relations. The presented model is capable of reproducing the transient behaviors observed in the experimental signal responses with multistep injection-purge cycles, including drifts and/or changes in the baseline. Moreover, this model can be utilized for extracting viscoelastic properties of the receptor material/analyte pairs as well as the concentrations of analytes accurately by fitting a couple of injection-purge curves obtained from the experimental data. The parameters of the model that best fit the data can be used for predicting the entire signal response.

I. INTRODUCTION

Nanomechanical sensors have gained significant attention as powerful tools for detecting target analytes,[1–7] especially odors that are composed of a complex mixture of gaseous molecules.[8–11] An array of nanomechanical sensors can be potentially used as a sensing unit for artificial olfaction. In the case of so-called static mode operation, sensing signals are obtained by measuring mechanical stress/strain induced by the sorption of target molecules in a receptor layer designed to respond to a wide range of chemical classes. Since such a multidimensional dataset obtained by a nanomechanical sensor array contains a large amount of information, multivariate analyses and machine learning can be effectively applied to distinguish and identify each specimen. To obtain highly accurate identification of target analytes by using pattern recognition-based analyses, there are various methods to extract the effective features from the multidimensional dataset.[12] However, most of the feature extraction methods are generally based on the empirical and/or mathematical interpretations and are not necessarily related to the scientific interpretation, such as the physical/chemical mechanism that is involved in the nanomechanical sensing.

Nanomechanical sensors are coated with a receptor layer that absorbs the analyte. Sorption-induced bending of metal-coated microcantilevers has been extensively studied.[13,14] The responses

from metal-coated cantilever-type nanomechanical sensors exhibit a first-order behavior representing an elastic behavior. In contrast to the elastic metal coating, polymers are often used as a coating material because polymers can be easily designed to respond to a large variety of chemical classes. Polymers often show viscoelastic behaviors, and hence the dynamic behaviors of nanomechanical sensing reflect the sorption kinetics along with the viscoelastic stress relaxation. For theoretical investigations, Wenzel *et al.*[15] proposed an analytical solution of dynamic responses of cantilever-type nanomechanical sensors coated with a viscoelastic material for a rectangular injection-purge system; it is possible to predict the viscoelastic signal responses using the parameters that describe the steady-state elongation and the sorption time. Imamura *et al.*[16] recently reported the effective feature extraction method by using Wenzel's theoretical model for analyte identification. In this model, it was assumed that the signal response reaches a steady-state. However, some of the signal responses do not reach a steady-state even after 1 h [Fig. 1(a)], probably due to the secondary and tertiary viscoelastic behaviors.[17] In such a case, it is difficult to extract the accurate viscoelastic features, and also a long time duration limits the applicability of nanomechanical sensors to practical artificial olfaction.

To measure a signal response with a relatively short duration in a practical condition,[18–20] the injection-purge cycle is often repeated [Figs. 1(b) and 1(c)], which is similar to inhalation–exhalation cycles of the human nose. By using the dataset obtained from the latter cycles, it is possible to identify various target analytes.[4–6,8–10] This

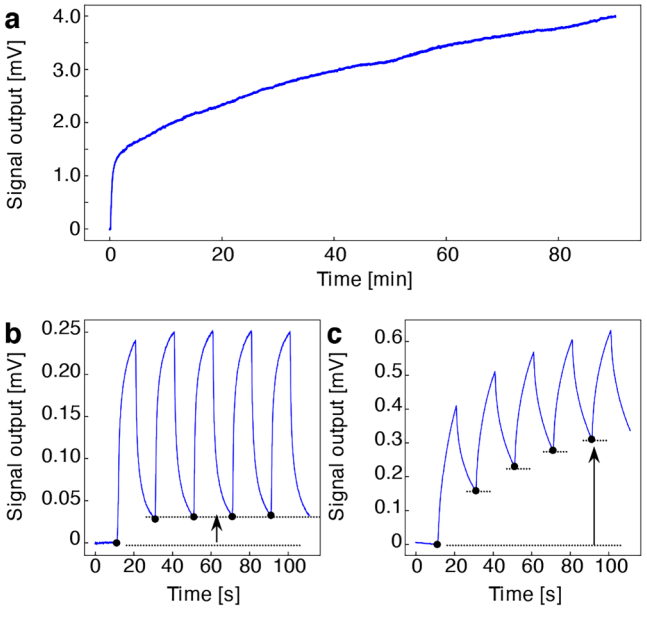

FIG. 1. Typical signal outputs measured by viscoelastic material-coated MSS. (a) Long time injection (90 min) of 10% *n*-dodecane to PS-coated MSS. (b) and (c) Multistep injection-purge cycle with duration time $T = 10$ s. Water (10%)/PCL (b) and *n*-dodecane (10%)/PS are shown. Black arrows denote the baseline drift.

multistep injection-purge cycle with a relatively short duration can minimize the effects induced by the long-time injection process [Fig. 1(a)], such as secondary and tertiary viscoelastic behaviors.[17] However, it frequently suffers from a severe drift of signal responses and/or change in their baseline [Fig. 1(c)], preventing the measurements of the reproducible signal responses. Although these phenomena must relate to the sorption of analytes into a receptor layer and subsequent release, an analytical expression of comprehensively describing the phenomena is still missing.

In the present study, we derive a general analytical expression that includes the sorption kinetics and the viscoelastic stress relaxation. This model is applicable to the multistep injection-purge cycles without reaching a steady-state, allowing us to effectively analyze the sensor response even if it drifts and/or changes its baseline over time. On the basis of the theoretical model proposed by Wenzel *et al.*,[15] we formulated a new model by deriving analytical solutions of overall transient (and steady-state) responses with multistep injection-purge cycles. This analytical model agrees well with sensor responses experimentally measured using a nanomechanical Membrane-type Surface stress Sensor (MSS)[3] coated with viscoelastic materials because of the high robustness and high sensitivity of MSS.[4,21] The curve fitting provides not only several physical parameters but also analyte concentration that can be utilized as solid features for scientifically reliable pattern recognition-based analyses.[8–10]

II. EXPERIMENTAL SECTION

A. Materials

Polystyrene (PS), polycaprolactone (PCL), and poly(4-methylstyrene) (P4MS) were purchased from Sigma-Aldrich. Alkyl-functionalized inorganic nanoparticles (octadecyl-functionalized silica/titania-based hybrid nanoparticles; C_{18}-STNPs) are fabricated according to our previous papers.[9,22] *N,N*-dimethylformamide (DMF), used as a solvent to prepare polymer solutions for inkjet spotting, was purchased from Wako Pure Chemical Industries. Ethanol, *n*-dodecane, and 1,2-dichlorobenzene (analytical or higher grade) used as solvent vapors were purchased from Wako Pure Chemical Industries, Nacalai tesque, and Sigma-Aldrich, respectively. All chemicals were used as purchased. MilliQ water (Merck MilliPore) was used to obtain water vapor.

B. Fabrication of MSS

The construction of the MSS chips and its working principle has been previously reported.[3,21] Briefly, MSS consists of a silicon-based membrane suspended by four piezoresistive beams, composing a full Wheatstone bridge [Fig. 2(a)]. The membrane is coated with a receptor material, which generates the surface stress caused by the sorption-induced expansion. The surface stress on the membrane is transduced to the four sensing beams as amplified uniaxial stress, resulting in the changes in the electrical resistance of the piezoresistors embedded in the beams. In contrast to simple cantilever-type nanomechanical sensors, in which a displacement of free-end Δz corresponds to a sensing signal, the signal output of MSS (V_{out}) is provided by the total output resistance change

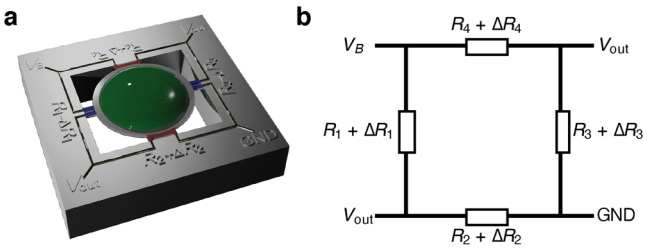

FIG. 2. Structure of the membrane-type surface stress sensor (MSS). (a) Three-dimensional schematic image of MSS structure. (b) Circuit diagram of the MSS.

obtained from the Wheatstone bridge circuit; it can be expressed as

$$V_{\text{out}} = \frac{V_B}{4}\left(\frac{\Delta R_1}{R_1} - \frac{\Delta R_2}{R_2} + \frac{\Delta R_3}{R_3} - \frac{\Delta R_4}{R_4}\right), \quad (1)$$

where V_B is the bridge voltage applied to the Wheatstone bridge circuit and $\Delta R_i/R_i$ is the relative resistance change in each sensing beam [Fig. 2(b)].

The receptor materials were coated directly onto the MSS membrane using an inkjet spotting (LaboJet-500SP, Microjet Co. Ltd.) equipped with a nozzle (IJHBS-300, Microjet Corporation). Each receptor material was dissolved in DMF at a concentration of 1 mg mL^{-1}, and the resulting solutions were deposited onto each channel of the MSS. The injection speed, volume of a droplet, and numbers of inkjet shots were fixed at ca. 5 m s^{-1}, ca. 300 pL, and 300 shots, respectively. A stage of the inkjet spotter was heated at 80 °C to promote evaporation of DMF. In the present study, we used viscoelastic material-coated MSS with more than 6-month aging to obtain reproducible signal responses.

C. Sensing

The coated MSS chips were placed in a Teflon chamber, which was placed in an incubator with a controlled temperature of 25.00 ± 0.02 °C. The chamber was connected to a gas system consisting of two mass flow controllers (MFCs), a mixing chamber, a purging gas line, and a vial for a solvent liquid. The vapor of each solvent was produced by bubbling carrier gas. Pure nitrogen gas was used as carrier and purging gases. The total flow rate was maintained at 100 mL min^{-1} during the experiments. The duration time was precisely controlled and the concentrations of the four different solvent vapors were controlled using MFC-1 at P_a/P_o of 0.1, 0.2, and 0.3, where P_a and P_o denote the partial vapor pressure and saturated vapor pressure of the solvent, respectively. Before measuring MSS signals, pure nitrogen gas was introduced into the MSS chamber for 1 min. Subsequently, MFC-1 (injection line) was switched on/off at each duration time T [s] with a controlled total flow rate of 100 mL min^{-1} using MFC-2 for up to 20 injection-purge cycles. Data were measured with a bridge voltage of −0.5 V and recorded with a sampling rate of 100 Hz. The data collection program was designed using LabVIEW (NI Corporation).

D. Curve fitting and estimation of parameters

To extract coating film properties from experimental data, we used least squares methods with trust region reflective algorithm using Python 3 with SciPy module. The bounds for each parameter were set at $\gamma \cdot \sigma_{\text{sat.}} > 0$, $E_U/E_R > 0$, $\tau_s > 0$, $\tau_r > 0$, and $10 \le t_0 \le 13$. The amplitude constant $\sigma_{\text{sat.}}$, the diffusion time constant τ_s, the relaxation time constant τ_r, and the ratio of unrelaxed and relaxed moduli E_U/E_R in addition to the time when the first injection starts (t_0) were optimized using the derived formula in the present study. The initial fitting parameters are set as follow: $\gamma \cdot \sigma_{\text{sat.}} = y_{\max} - y_{\min}$, $E_U/E_R = 5$, $\tau_s = 100$ [s], $\tau_r = 6$ [s], and $t_0 = 11$ [s], where $y_{\max}$ and $y_{\min}$ are the maximum and minimum values of each signal response.

III. BACKGROUND THEORY

First, we summarize the background theory used to calculate the sorption-induced and concentration-dependent nanomechanical sensing models for elastic and viscoelastic materials, respectively, using a rectangular injection sequence as illustrated in Fig. 3. A more detailed discussion of the background theory is given in the literature reported by Wenzel *et al.*[15]

A. Sorption-induced nanomechanical sensing

When a receptor material coated on a nanomechanical sensor is exposed to a chemical analyte, the receptor material expands owing to the sorption-induced deformation. However, the receptor material is attached to a substrate and is not free to expand. In the

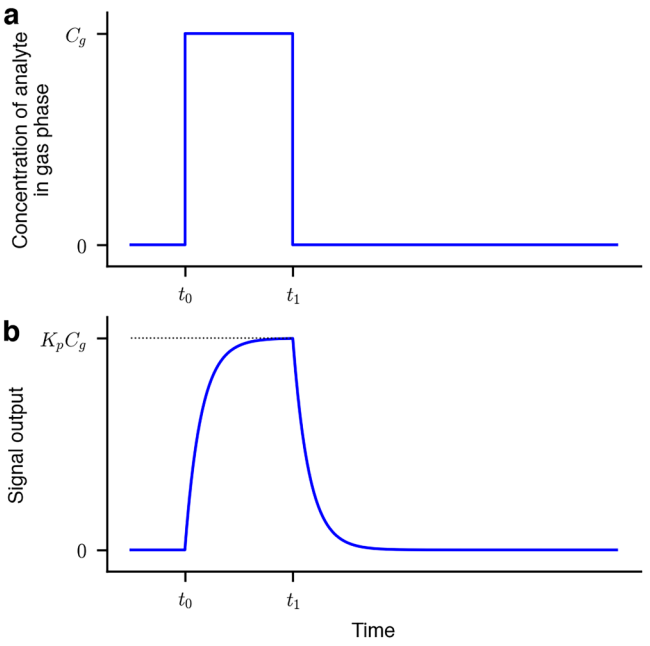

FIG. 3. Rectangular injection. (a) Rectangular analyte injection. (b) Typical signal output.

case of so-called static mode operation of a microcantilever plate, the sorption-induced expansion makes the cantilever beam bend.[1] Several analytical solutions have been proposed for the theoretical formulation of the static mode operation of nanomechanical sensing, especially for a microcantilever model. For example, the displacement of a free-end of a cantilever Δz induced by isotropic internal strain in a receptor layer ε_f is given by[23]

$$\Delta z = \frac{3l^2(h_f + h_s)}{(A+4)h_f^2 + (A^{-1}+4)h_s^2 + 6h_f h_s}\varepsilon_f, \tag{2}$$

with

$$A = \frac{E_f w_f h_f}{1-\nu_f} \Big/ \frac{E_s w_s h_s}{1-\nu_s}, \tag{3}$$

where the subscripts "f" and "s" denote the coating film and the cantilever substrate, respectively; l, h, w, E, and ν represent the length, height, width, Young's modulus, and Poisson's ratio, respectively. The internal strain in a coating film ε_f can be replaced by other parameters, such as three-dimensional internal stress in the coating film σ_f ([N m^{-2}]) or two-dimensional surface stress σ_{surf} ([N m^{-1}]) using the relations $\varepsilon_f = \sigma(1-\nu_f)/E_f$ or $\sigma_f = \sigma_{\text{surf}}/h_f$.[23–25] When a cantilever is covered with a thin film having a same width (i.e., $h_f \ll h_s$ and $w_f = w_s$), Eq. (2) reduces to the following equation, which is known as Stoney's equation:[24]

$$\Delta z = \frac{3l^2(1-\nu_s)}{E_s h_s^2}\sigma_{\text{surf}}. \tag{4}$$

In the case of the sorption-induced nanomechanical sensing, there are several investigations using microcantilever sensors.[13,15] Wenzel *et al.* proposed the theoretical formulation of the dynamic behavior for a cantilever plate, especially for that coated with a viscoelastic material.[15] In this model, the sorption-induced internal strain in a coating film ε_f is approximated as follows: in the gas phase, the volume of a coating film $V(C)$, which is not attached to a cantilever substrate, changes with the concentration of an analyte in the coating film C (mol mL^{-1} of coating film) as

$$V(C) = V_0(1 + C\nu_a), \tag{5}$$

where V_0 is the initial volume of the coating film and ν_a is the specific volume of the absorbed analyte. Assuming that the coating film is isotropic and expands isotropically in all directions, the absorption-induced strain varies with concentration as

$$\varepsilon_f(C) = \sqrt[3]{1 + C\nu_a} - 1, \tag{6a}$$

which has the linear approximation given by

$$\varepsilon_f(C) = \frac{1}{3}C\nu_a \tag{6b}$$

for small volume expansion (i.e., $\varepsilon_f \ll 1$). The absorption-induced strain can, therefore, be assumed directly proportional to the absorbed analyte concentration. Let $\varepsilon_f(t) = \lambda C(t)$, where $\lambda = \frac{1}{3}\nu_a$; the deflection at the free-end of the cantilever $\Delta z(t)$ for the case described in Eq. (2) can be then given by

$$\Delta z(t) = \frac{3l^2(h_f + h_s)}{(A+4)h_f^2 + (A^{-1}+4)h_s^2 + 6h_f h_s}\lambda C(t). \tag{7}$$

Stoney's equation [Eq. (4)] can similarly be used to develop a simpler expression for $h_f \ll h_s$. Equation (7) relates the cantilever response to the sorbed analyte concentration $C(t)$ in the coating film. The expression indicates that the dynamic behavior of the absorption causes deflection. Thus, it is necessary to know how the absorbed analyte concentration in the coating film varies with time.

It should be noted that a signal response of MSS generally correlates with the internal strain, which is similar to the cantilever-type sensors.[26] In the present study, we used MSS for experimental investigation. Although no analytical solution is reported for the signal response of MSS, we have revealed that the resistance change of piezoresistive sensing beams of MSS reflects the linear correlation with the internal strain ε_f through experiments[4,6] and simulations using finite element analysis (FEA).[6,27–29] Therefore, the signal responses of MSS can also be assumed to be directly proportional to the absorbed analyte concentration as expressed in Eq. (7).

B. Governing equations for single-step absorption/desorption processes

For the derivation of the equations governing the concentration of an analyte A into a receptor material coated on a nanomechanical sensor during absorption/desorption processes, we assume a first-order absorption of A with absorption rate constant k_a and desorption rate constant k_d as

$$\text{A(g)} \underset{k_d}{\overset{k_a}{\rightleftharpoons}} \text{A(s)}, \tag{8}$$

where A(g) and A(s) denote an analyte in the gas phase and in coating film, respectively. The reaction rate of a concentration of an analyte in the coating film $C(t)$ is given by

$$\frac{d}{dt}C(t) = k_a \cdot C_g(t) - k_d \cdot C(t), \tag{9a}$$

where $C_g(t)$ is the concentration of analyte in the gas phase as a function of time. Although the absorption process of an analyte into a bulk of the coating film is generally rate limited by the diffusion of the analyte across the surface barrier and into the coating film,[13] this reaction rate is equivalent to the diffusion time constant τ_s reported by Wenzel *et al.*[15] as

$$\frac{d}{dt}C(t) = \frac{1}{\tau_s}\left[K_p C_g(t) - C(t)\right], \tag{9b}$$

where $\tau_s = 1/k_d$; $K_p = k_a/k_d$ is known as the partition coefficient in the case of a polymer coating film. We also use the time constant τ_s instead of the desorption rate constant k_d.

In the case of gas sensing using nanomechanical sensors, the sample gas is introduced by carrier gas (e.g., nitrogen); subsequently, the gas line is switched to the purge gas line (e.g., nitrogen) to promote the desorption of the sample gases. Since the injection of analyte is generally controlled by the continuous flow of headspace gas or bubbling liquid samples, it can be assumed to be homogeneous in time. Thus, a rectangular injection of analyte with constant rate can be considered as depicted in Fig. 3(a). When the analyte is injected at $t = t_0$ and maintained at a constant concentration C_g until the time to start the purge t_1, the concentration of analyte in the gas phase $C_g(t)$ can be considered as a step function:

$$C_g(t) = \begin{cases} 0, & t < t_0 \\ C_g, & t_0 \le t < t_1. \\ 0, & t_1 \le t \end{cases} \tag{10}$$

It is assumed that the initial concentration in the coating film $C(t)$ is zero before injection starts (i.e., $t < t_0$). Using Eq. (10), the reaction rate of A in the coating film [Eq. (9b)] can be described as a step function:

$$\frac{d}{dt}C(t) = \begin{cases} 0, & t < t_0 \\ \frac{1}{\tau_s}\left[K_p C_g - C(t)\right], & t_0 \le t < t_1. \\ -\frac{1}{\tau_s}\cdot C(t) & t_1 \le t \end{cases} \tag{11}$$

The general differential equations for the reaction rate during the absorption process (i.e., the injection process; $t_0 \le t < t_1$) and the desorption process (i.e., the purge process; $t \ge t_1$) can be solved as

$$C(t) = \begin{cases} 0 & t < t_0 \\ K_p C_g + C_1 \cdot e^{-\frac{t}{\tau_s}}, & t_0 \le t < t_1, \\ C_2 \cdot e^{-\frac{t}{\tau_s}}, & t_1 \le t \end{cases} \tag{12}$$

where C_1 and C_2 are the constants of integration.

Although Eq. (12) is a step function, the dynamic concentration in a coating film must be a continuous function. As for the boundary condition at $t = t_0$, the concentration of analyte in the coating film should be zero. Consequently, the constant of integration $C_1 = -K_p C_g \cdot e^{t_0/\tau_s}$. Substituting this into Eq. (12), the concentration of the analyte in the coating film can be obtained by

$$C(t) = K_p C_g\left(1 - e^{-\frac{t-t_0}{\tau_s}}\right), \quad t_0 \le t < t_1. \tag{13}$$

Subsequently, as a second boundary condition at the beginning of the desorption process ($t = t_1$), the concentration of analyte in the coating film should be equal to that at the end of the absorption process [Eq. (13)]. Thus, the constant C_2 can be solved as

$$C_2 = K_p C_g\left(1 - e^{-\frac{t_1-t_0}{\tau_s}}\right) \cdot e^{\frac{t_1}{\tau_s}}. \tag{14}$$

Substituting C_2 into Eq. (12), the particular solution of the differential equations can be solved. The concentration of the analyte in the coating film at any time t is given by

$$C(t) = \begin{cases} 0, & t < t_0 \\ K_p C_g\left(1 - e^{-\frac{t-t_0}{\tau_s}}\right), & t_0 \le t < t_1. \\ K_p C_g\left(1 - e^{-\frac{t_1-t_0}{\tau_s}}\right) \cdot e^{-\frac{t-t_1}{\tau_s}}, & t_1 \le t \end{cases} \tag{15a}$$

Let $T = t_1 - t_0$ be the duration time for injection; then the concentration of analyte A can be simplified as

$$C(t) = \begin{cases} 0, & t < t_0 \\ K_p C_g\left(1 - e^{-\frac{t-t_0}{\tau_s}}\right), & t_0 \le t < t_1. \\ K_p C_g\left(1 - e^{-\frac{T}{\tau_s}}\right) \cdot e^{-\frac{t-t_1}{\tau_s}}, & t_1 \le t \end{cases} \tag{15b}$$

The analytical solution of the absorption process can be expressed as a typical first-order response. As described above, when the coating film is an elastic material, the signal response of nanomechanical sensing can be assumed to be proportional to the concentration of the analyte in the coating film, if the sorption-induced expansion is small. Indeed, the typical signal outputs of an MSS are transduced from the sorption-induced expansion with the estimated internal strain ε_f in the range from approximately 1×10^{-6} simulated by FEA.[6,28]

C. Governing equations for viscoelastic materials

Among a large variety of materials, viscoelastic properties arise from dynamic differences on molecular rearrangements.[30] Wenzel *et al.* proposed a theoretical model for a cantilever-type nanomechanical sensor coated with a viscoelastic material.[15] The theoretical models are derived from the simplest three-parameter solid model:[15,31]

$$\tau_r E_U \frac{d}{dt}\varepsilon(t) + E_R\varepsilon(t) = \tau_r \frac{d}{dt}\sigma(t) + \sigma(t), \tag{16}$$

where E_U and E_R denote the unrelaxed (instantaneous) modulus and the relaxed (asymptotic) modulus, respectively, and τ_r is the time constant of stress relaxation. The three-parameter solid model describes the stress/strain relationship in a viscoelastic solid that exhibits both viscous and elastic properties. As proposed by Wenzel *et al.*,[15] the derived general differential equations from Eq. (16) can be greatly simplified as

$$\frac{d}{dt}\sigma(t) = -\frac{\sigma(t)}{\tau_r} + \frac{E_R\lambda}{\tau_s}\left(\frac{E_U}{E_R} - \frac{\tau_s}{\tau_r}\right)C(t) - \frac{E_U K_p \lambda}{\tau_s}C_g(t), \tag{17}$$

when the coating film is significantly soft (i.e., $E_U \ll E_s$) or thin (i.e., $h_f \ll h_s$). In the case of MSS, the membrane (substrate) is made of silicon (approximately 170 GPa). In general, the substrate material is considerably stiffer than the polymer materials, whose unrelaxed moduli are usually in the range from 10 MPa to 5 GPa. Accordingly, the general differential equation in Eq. (17) can be utilized in the present study.

For derivation of the equations governing the stress with a rectangular injection, we again consider the step function of the concentration of analyte in the gas phase $C_g(t)$ in Eq. (10). Substituting Eqs. (10) and (15a) into Eq. (17), the general differential equation of stress can be described as a step function:

$$\frac{d}{dt}\sigma(t) = \begin{cases} 0, & t < t_0 \\ -\dfrac{\sigma(t)}{\tau_r} - \dfrac{\sigma_{\text{sat.}}}{\tau_s}\left(\dfrac{E_U}{E_R} - \dfrac{\tau_s}{\tau_r}\right)e^{-\frac{t-t_0}{\tau_s}} - \dfrac{\sigma_{\text{sat.}}}{\tau_r}, & t_0 \le t < t_1, \\ -\dfrac{\sigma(t)}{\tau_r} + \dfrac{\sigma_{\text{sat.}}}{\tau_s}\left(\dfrac{E_U}{E_R} - \dfrac{\tau_s}{\tau_r}\right)\left(1 - e^{-\frac{t_1-t_0}{\tau_s}}\right)e^{-\frac{t-t_1}{\tau_s}}, & t_1 < t \end{cases} \tag{18}$$

with

$$\sigma_{\text{sat.}} = E_R \lambda K_p C_g. \tag{19}$$

$\sigma_{\text{sat.}}$ denotes the stress at the saturated or the equilibrium state. The general differential equations of the stresses during the absorption and desorption processes can be solved as

$$\sigma(t) = \begin{cases} \sigma_0, & t < t_0 \\ -\sigma_{\text{sat.}} + \sigma_{\text{sat.}}\alpha \cdot e^{-\frac{t-t_0}{\tau_s}} + C_3 \cdot e^{-\frac{t}{\tau_r}}, & t_0 \le t < t_1, \\ -\sigma_{\text{sat.}}\alpha\left(1 - e^{-\frac{t_1-t_0}{\tau_s}}\right) \cdot e^{-\frac{t-t_1}{\tau_s}} + C_4 \cdot e^{-\frac{t}{\tau_r}}, & t_1 \le t \end{cases} \tag{20}$$

with

$$\alpha = \frac{1}{\tau_s}\left(\frac{E_U}{E_R} - \frac{\tau_s}{\tau_r}\right)\left(\frac{1}{\tau_s} - \frac{1}{\tau_r}\right)^{-1}, \tag{21}$$

where C_3 and C_4 are the constants of integration.

During rectangular injection-purge, again the stresses must be a continuous function. As for the boundary condition at the beginning of the absorption process, the stress must be σ_0. Then, C_3 can be solved as

$$C_3 = \sigma_{\text{sat.}}(1-\alpha) \cdot e^{\frac{t_0}{\tau_r}} + \sigma_0 \cdot e^{\frac{t_0}{\tau_r}}. \tag{22}$$

The substitution of C_3 into Eq. (20) yields the stress of the absorption process as

$$\sigma(t) = -\sigma_{\text{sat.}} + \sigma_{\text{sat.}}\alpha \cdot e^{-\frac{t-t_0}{\tau_s}} + \sigma_{\text{sat.}}(1-\alpha) \cdot e^{-\frac{t-t_0}{\tau_r}} + \sigma_0 \cdot e^{-\frac{t-t_0}{\tau_r}}. \tag{23}$$

From Eq. (23), the second boundary condition of the stress at the beginning of purge can be estimated. The constant C_4 is, therefore, given by

$$C_4 = \sigma_0 e^{\frac{t_0}{\tau_r}} - \sigma_{\text{sat.}}(1-\alpha)\left(1 - e^{-\frac{t_1-t_0}{\tau_r}}\right) \cdot e^{\frac{t_1}{\tau_r}}. \tag{24}$$

Substituting C_4 into Eq. (20), the particular solutions of the differential equations can be solved and the stress at any time t can be obtained as follows:

$$\sigma(t) = \begin{cases} \sigma_0, & t < t_0 \\ -\sigma_{\text{sat.}} + \sigma_{\text{sat.}}\alpha \cdot e^{-\frac{t-t_0}{\tau_s}} + \sigma_0 \cdot e^{-\frac{t-t_0}{\tau_r}} + \sigma_{\text{sat.}}(1-\alpha) \cdot e^{-\frac{t-t_0}{\tau_r}}, & t_0 \le t < t_1. \\ -\sigma_{\text{sat.}}\alpha\left(1 - e^{-\frac{t_1-t_0}{\tau_s}}\right) \cdot e^{-\frac{t-t_1}{\tau_s}} + \sigma_0 \cdot e^{-\frac{t-t_0}{\tau_r}} - \sigma_{\text{sat.}}(1-\alpha)\left(1 - e^{-\frac{t_1-t_0}{\tau_r}}\right) \cdot e^{-\frac{t-t_1}{\tau_r}}, & t_1 \le t \end{cases} \tag{25}$$

Although the resulting stresses in Eq. (25) are given in negative values, the original definition proposed by Wenzel *et al.*[15] states that the positive z is directed downward of a cantilever plate; thus, the corresponding analytical solution of the deflection at the free-end of the cantilever is also multiplied by negative one, as can be seen in Eq. (20b) in Ref. 15. It should be noted that we use the equations multiplied by negative one to apply the analytical solutions of viscoelastic models to the MSS with the same directions of surface stress; a positive sign corresponds to the initial compressive stress and vice versa.

It should also be noted that when the signal reaches the steady-state or equilibrium state, the stresses in Eq. (25) can be further simplified and be equivalent to Eqs. (11b) and (12b) in Ref. 16, if $\sigma_0 = 0$. In the simplified equations for the steady-state, the rising and decay curves become symmetric.

IV. ANALYTICAL SOLUTIONS

In nanomechanical sensing, the multistep injection-purge cycles are often used to obtain the repetitive signal patterns to extract multistep sets of features for the pattern recognition (Fig. 1).[4–6,8–10,32] However, the signal output is sometimes obtained with monotonous increase in the baseline as depicted in Figs. 1(b) and 1(c). This can be due to the asymmetric nature between the absorption and desorption processes, even the desorption rate constant is the same as k_d or equivalently $1/\tau_s$. In the present study, using the above theoretical framework, we now derive the analytical solutions of the dynamic concentrations of the analyte in the receptor materials with viscoelastic properties at the n-th injection and purge processes.

A. Concentrations of analyte at *n*-th injection and purge

For the multistep injection-purge cycles, we consider a rectangular pulse wave-like sequence (Fig. 4). The concentration of an analyte in the gas phase $C_g(t)$ can be described as a step function:

$$C_g(t) = \begin{cases} 0, & t < t_0 \\ C_g, & t_{2(n-1)} \le t < t_{2n-1}, \\ 0, & t_{2n-1} \le t < t_{2n} \end{cases} \tag{26}$$

$$n = 1, 2, \ldots.$$

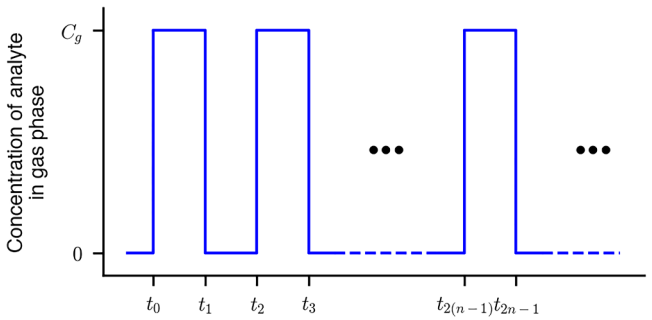

FIG. 4. Rectangular pulse wave-like gas injection.

Let ${}^{\text{inj.}}C_n(t)$ and ${}^{\text{purg.}}C_n(t)$ be the concentrations of analyte in a coating film at the n-th injection and at n-th purge, respectively. Then, the reaction rate can be described as a step function:

$$\begin{cases} \dfrac{d}{dt}C(t) = 0, & t < t_0 \\ \dfrac{d}{dt}{}^{\text{inj.}}C_n(t) = \dfrac{1}{\tau_s}\left[K_pC_g - {}^{\text{inj.}}C_n(t)\right], & t_{2(n-1)} \le t < t_{2n-1}, \\ \dfrac{d}{dt}{}^{\text{purg.}}C_n(t) = -\dfrac{1}{\tau_s}{}^{\text{purg.}}C_n(t), & t_{2n-1} \le t < t_{2n} \end{cases} \tag{27}$$

$n = 1, 2, \ldots.$

In the n-th purge process (i.e., $2n$-th step), the general differential equation can be solved as

$${}^{\text{inj.}}C_n(t) = K_pC_g + {}^{\text{inj.}}C_n \cdot e^{-\frac{t}{\tau_s}},\ t_{2(n-1)} \le t < t_{2n-1}, \tag{28a}$$

$${}^{\text{purg.}}C_n(t) = {}^{\text{purg.}}C_n \cdot e^{-\frac{t}{\tau_s}},\ t_{2n-1} \le t < t_{2n}, \tag{28b}$$

where ${}^{\text{inj.}}C_n$ and ${}^{\text{purg.}}C_n$ are the arbitrary constants of the n-th injection and purge, respectively. The concentration at the beginning of the n-th purge can be estimated using the concentration of the n-th injection process [i.e., $(2n-1)$-th step] as ${}^{\text{inj.}}C_n(t_{2n-1})$. From Eq. (28b), the concentration of n-th purge can be obtained as

$${}^{\text{purg.}}C_n(t) = {}^{\text{inj.}}C_n(t_{2n-1}) \cdot e^{-\frac{t-t_{2n-1}}{\tau_s}}. \tag{29}$$

Similarly, the concentration at the beginning of the $(n+1)$-th injection process (i.e., $t = t_{2n}$) should be the concentration at the end of the n-th purge process. From Eqs. (28a) and (29), the concentration of the $(n+1)$-th injection, therefore, can be found as

$${}^{\text{inj.}}C_{n+1}(t) = K_pC_g\left(1 - e^{-\frac{t-t_{2n}}{\tau_s}}\right) + {}^{\text{inj.}}C_n(t_{2n-1}) \cdot e^{-\frac{t_{2n-1}}{\tau_s}}. \tag{30}$$

Again, owing to the connectivity of the dynamic concentration behavior between at the end of the purge and at the beginning of the injection, the concentration of the $(n+1)$-th purge process can be obtained from Eqs. (28b) and (30) as follows:

$${}^{\text{purg.}}C_{n+1}(t) = K_pC_g\left(e^{-\frac{t-t_{2n+1}}{\tau_s}} - e^{-\frac{t-t_{2n}}{\tau_s}}\right) + {}^{\text{inj.}}C_n(t_{2n-1}) \cdot e^{-\frac{t-t_{2n-1}}{\tau_s}}. \tag{31}$$

From Eqs. (29) and (31), the recurrence relation of the concentration between the n-th and $(n+1)$-th purges and that between $(n+1)$-th injection and n-th purge can be found by

$${}^{\text{purg.}}C_{n+1}(t) - {}^{\text{purg.}}C_n(t) = K_pC_g\left(e^{-\frac{t-t_{2n+1}}{\tau_s}} - e^{-\frac{t-t_{2n}}{\tau_s}}\right), \tag{32a}$$

$${}^{\text{inj.}}C_{n+1}(t) - {}^{\text{purg.}}C_n(t) = K_pC_g\left(1 - e^{-\frac{t-t_{2n}}{\tau_s}}\right), \tag{32b}$$

respectively, with the concentration at the first purge is given in Eq. (15a) as

$${}^{\text{purg.}}C_1(t) = K_pC_g\left(e^{-\frac{t-t_1}{\tau_s}} - e^{-\frac{t-t_0}{\tau_s}}\right). \tag{32c}$$

Thus, the recurrence formula can be solved, and hence the concentration at the n-th injection and purge processes can be obtained as

$${}^{\text{inj.}}C_n(t) = K_pC_g - K_pC_g \cdot e^{-\frac{t}{\tau_s}}\sum_{i=0}^{2(n-1)}(-1)^i e^{\frac{t_i}{\tau_s}}, \tag{33a}$$

$${}^{\text{purg.}}C_n(t) = -K_pC_g \cdot e^{-\frac{t}{\tau_s}}\sum_{i=0}^{2n-1}(-1)^i e^{\frac{t_i}{\tau_s}}. \tag{33b}$$

It should be noted that the derived n-th injection and purge concentrations in Eq. (33) can be further simplified when the duration of injection and purge are fixed at T (i.e., $T = t_{2n} - t_{2n-1} = t_{2n-1} - t_{2(n-1)}$). Because $t_n - t_0 = n \cdot T$, multiplying the right-hand side of Eq. (33) by $(e^{-t_0/\tau_s} \cdot e^{t_0/\tau_s})$, the concentrations can be modified as

$${}^{\text{inj.}}C_n(t) = K_pC_g - K_pC_g \cdot e^{-\frac{t-t_0}{\tau_s}}\sum_{i=0}^{2(n-1)}\left(-e^{\frac{T}{\tau_s}}\right)^i \tag{34a}$$

$$= K_pC_g - K_pC_g \cdot e^{-\frac{t-t_{2(n-1)}}{\tau_s}}\sum_{i=0}^{2(n-1)}\left(-e^{-\frac{T}{\tau_s}}\right)^i, \tag{34b}$$

$$t_{2(n-1)} \le t < t_{2n-1},$$

$${}^{\text{purg.}}C_n(t) = -K_pC_g \cdot e^{-\frac{t-t_0}{\tau_s}}\sum_{i=0}^{2n-1}\left(-e^{\frac{T}{\tau_s}}\right)^i \tag{35a}$$

$$= K_pC_g \cdot e^{-\frac{t-t_{2n-1}}{\tau_s}}\sum_{i=0}^{2n-1}\left(-e^{-\frac{T}{\tau_s}}\right)^i, \tag{35b}$$

$$t_{2n-1} \le t < t_{2n}.$$

The models given in Eqs. (34) and (35) are assumed to be proportional to the concentration of analyte in gas phase C_g; additionally,

K_pC_g is related to the amplitude of the signal. In Eqs. (34b) and (35b), the terms t_{2n-1} and $t_{2(n-1)}$ denote the time when the signal starts to rise and to decay for each step in the rectangular pulse wave-like injection-purge cycles, respectively. Since the signal output of the nanomechanical sensing is directly proportional to the concentration $C(t)$ as described in Sec. III A [Eq. (7)], the signal output is analytically derived for the rectangular injection-purge cycles.

In Eqs. (34) and (35), if the duration T is long enough (i.e., the signal reaches equilibrium state), the term $e^{-n\cdot T/\tau_s}$ is negligible; then, the models given in Eqs. (34) and (35) are symmetric injection-purge curves as follows:

$$^{\text{inj.}}C_n(t) = K_pC_g - K_pC_g \cdot e^{-\frac{t-t_{2(n-1)}}{\tau_s}},\ t_{2(n-1)} \le t < t_{2n-1}, \tag{36a}$$

$$^{\text{purg.}}C_n(t) = K_pC_g \cdot e^{-\frac{t-t_{2n-1}}{\tau_s}},\qquad t_{2n-1} \le t < t_{2n}. \tag{36b}$$

In contrast, when the duration T is short or the desorption time constant τ_s is slow, the signal gives asymmetric curves, leading to an increase in the baseline as shown in Fig. 5. Note that the signal reaches symmetric patterns upon increasing the injection-purge cycles due to $\lim_{n\to\infty} e^{-n\cdot T/\tau_s} = 0$ [Fig. 5(b)]. The model clearly indicates that the analyte with fast τ_s desorbs from the coating film while the analyte with slow τ_s accumulates in the coating film when duration time T is relatively short [Fig. 5(a); e.g., $\tau_s = 120$].

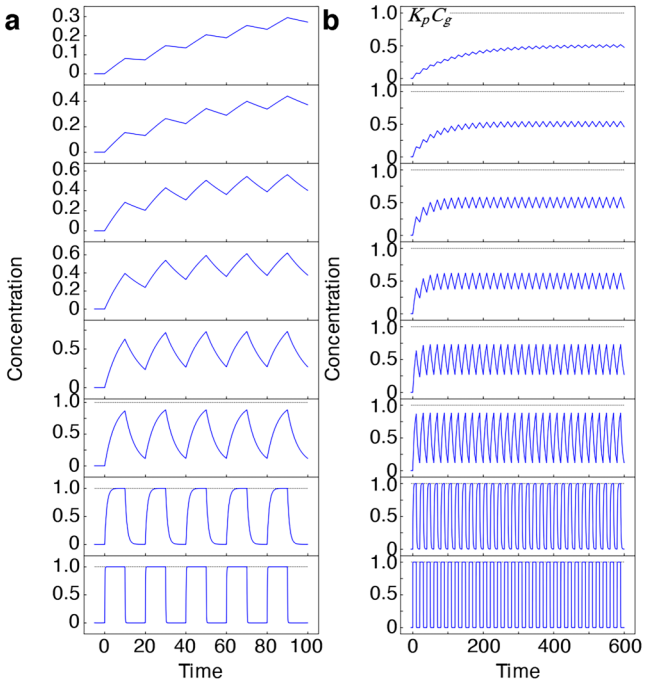

FIG. 5. Dynamic variation of an analyte concentration in a coating film estimated by Eqs. (34) and (35). The numbers of injection-purge cycles is 5 (a) and 30 (b). τ_s is varied with 120, 60, 30, 20, 10, 5, 1, and 0.1 from the top to bottom, and other parameters are fixed; $K_p = 1$; $C_g = 1$; $T = 10$; and $t_0 = 0$. All black dashed lines are the level of the amplitude K_pC_g, while the black dashed lines in the top five graph of (a) are not shown because of out of range.

B. Stress with viscoelastic materials at *n*-th injection and purge

We derived the concentration of analyte A in the coating film at the n-th injection and purge in Eq. (33). According to the formulation derived by Wenzel *et al.*,[15] the derived general differential equations of stress in Eq. (17) can be extended to the rectangular pulse wave-like injection models. Substituting Eq. (27) into Eq. (17) with Eq. (26), the general differential equations of stress can be rewritten at the n-th injection and purge as a step function, and can be solved as

$$^{\text{inj.}}\sigma_n(t) = -\sigma_{\text{sat.}} + \sigma_{\text{sat.}}\alpha \cdot e^{-\frac{t}{\tau_s}} \sum_{i=0}^{2(n-1)} (-1)^i e^{\frac{t_i}{\tau_s}} + {}^{\text{inj.}}C_n^{\sigma} \cdot e^{-\frac{t}{\tau_r}},$$
$$t_{2(n-1)} \le t < t_{2n-1}, \tag{37a}$$

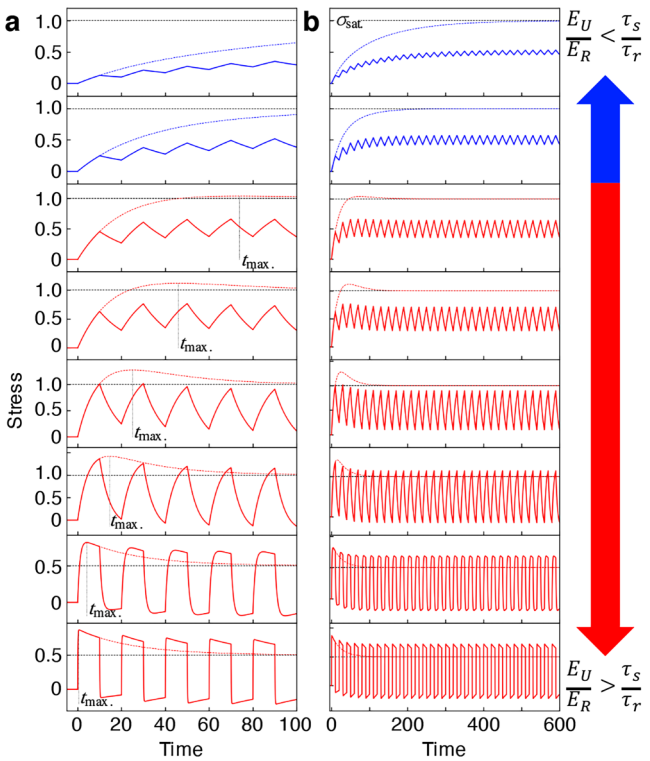

FIG. 6. Dynamic stress change derived from sorption-induced deformation estimated by Eqs. (44) and (45). The numbers of injection-purge cycles are 5 (a) and 30 (b). τ_s is varied with 120, 60, 30, 20, 10, 5, 1, and 0.1 from top to bottom, and other parameters are fixed; $E_U/E_R = 1.75$; $\tau_r = 25$ [s]; $\sigma_{\text{sat.}} = 1$; and $t_0 = 0$. Solid lines and dashed lines for the stress change denote the duration time $T = 10$ and >600 [s], respectively. All black dashed horizontal lines are the level of the amplitude $\sigma_{\text{sat.}}$. Black vertical dotted lines are the time when an overshoot starts to decay $t_{\text{max.}}$.

$$ {}^{\text{purg.}}\sigma_n(t) = \sigma_{\text{sat.}}\alpha \cdot e^{-\frac{t}{\tau_s}} \sum_{i=0}^{2n-1} (-1)^i e^{\frac{t_i}{\tau_s}} + {}^{\text{purg.}}C_n^{\sigma} \cdot e^{-\frac{t}{\tau_r}}, \quad t_{2n-1} \le t < t_{2n}, \tag{37b} $$

where ${}^{\text{inj.}}\sigma_n(t)$ and ${}^{\text{purg.}}\sigma_n(t)$ denote the stress at the n-th injection and purge, respectively; ${}^{\text{inj.}}C_n^{\sigma}$ and ${}^{\text{purg.}}C_n^{\sigma}$ are the arbitrary constants of the n-th injection and purge, respectively.

As the boundary condition, the stress at the beginning of the n-th purge process should be ${}^{\text{inj.}}\sigma_n(t_{2n-1})$. From Eq. (37) with ${}^{\text{inj.}}\sigma_n(t_{2n-1})$, the stress of the n-th purge process can be obtained by

$$ {}^{\text{purg.}}\sigma_n(t) = \sigma_{\text{sat.}}\alpha \cdot e^{-\frac{t}{\tau_s}} \sum_{i=0}^{2n-1} (-1)^i e^{\frac{t_i}{\tau_s}} + a_n, \tag{38} $$

with

$$ a_n = \left[{}^{\text{inj.}}\sigma_n(t_{2n-1}) - \sigma_{\text{sat.}}\alpha \cdot e^{-\frac{t_{2n-1}}{\tau_r}} \sum_{i=0}^{2n-1} (-1)^i e^{\frac{t_i}{\tau_s}} \right] e^{-\frac{t-t_{2n-1}}{\tau_r}}. $$

Similarly, from the boundary conditions at the beginning of the $(n+1)$-th injection and purge processes, the stresses can also be written using ${}^{\text{inj.}}\sigma_n(t_{2n-1})$ as

$$ {}^{\text{inj.}}\sigma_{n+1}(t) = -\sigma_{\text{sat.}} + \sigma_{\text{sat.}}\alpha \cdot e^{-\frac{t}{\tau_s}} \sum_{i=0}^{2n} (-1)^i e^{\frac{t_i}{\tau_s}} + \sigma_{\text{sat.}}(1-\alpha) \cdot e^{-\frac{t-t_{2n}}{\tau_r}} + a_n, \tag{39} $$

$$ {}^{\text{purg.}}\sigma_{n+1}(t) = \sigma_{\text{sat.}}\alpha \cdot e^{-\frac{t}{\tau_s}} \sum_{i=0}^{2n+1} (-1)^i e^{\frac{t_i}{\tau_s}} + \sigma_{\text{sat.}}(1-\alpha)\left(e^{\frac{t_{2n}}{\tau_r}} - e^{\frac{t_{2n+1}}{\tau_r}}\right) \cdot e^{-\frac{t}{\tau_r}} + a_n. \tag{40} $$

From the recurrence relations of the stress between the n-th and $(n+1)$-th purge and that between the $(n+1)$-th injection and n-th purge processes in Eqs. (38)–(40) with Eq. (25), the recurrence formula of the stress can be found as

$$ {}^{\text{purg.}}\sigma_{n+1}(t) - {}^{\text{purg.}}\sigma_n(t) = \sigma_{\text{sat.}}\alpha \cdot e^{-\frac{t}{\tau_s}}\left(e^{\frac{t_{2n}}{\tau_s}} - e^{\frac{t_{2n+1}}{\tau_s}}\right) + \sigma_{\text{sat.}}(1-\alpha) \cdot e^{-\frac{t}{\tau_r}}\left(e^{\frac{t_{2n}}{\tau_r}} - e^{\frac{t_{2n+1}}{\tau_r}}\right), \tag{41a} $$

$$ {}^{\text{inj.}}\sigma_{n+1}(t) - {}^{\text{purg.}}\sigma_n(t) = -\sigma_{\text{sat.}} + \sigma_{\text{sat.}}\alpha \cdot e^{-\frac{t-t_{2n}}{\tau_s}} + \sigma_{\text{sat.}}(1-\alpha)e^{-\frac{t-t_{2n}}{\tau_r}}. \tag{41b} $$

The recurrence formula can be solved, and hence the stress at the n-th injection and purge processes can be obtained as

$$ {}^{\text{inj.}}\sigma_n(t) = -\sigma_{\text{sat.}} + \sigma_{\text{sat.}}\alpha \cdot e^{-\frac{t}{\tau_s}} \sum_{i=0}^{2(n-1)} (-1)^i e^{\frac{t_i}{\tau_s}} + \sigma_{\text{sat.}}(1-\alpha) \cdot e^{-\frac{t}{\tau_r}} \sum_{i=0}^{2(n-1)} (-1)^i e^{\frac{t_i}{\tau_r}} + \sigma_0 \cdot e^{-\frac{t-t_0}{\tau_r}}, \quad t_{2(n-1)} \le t < t_{2n-1}, \tag{42} $$

$$ {}^{\text{purg.}}\sigma_n(t) = \sigma_{\text{sat.}}\alpha \cdot e^{-\frac{t}{\tau_s}} \sum_{i=0}^{2n-1} (-1)^i e^{\frac{t_i}{\tau_s}} + \sigma_{\text{sat.}}(1-\alpha) \cdot e^{-\frac{t}{\tau_r}} \sum_{i=0}^{2n-1} (-1)^i e^{\frac{t_i}{\tau_r}} + \sigma_0 \cdot e^{-\frac{t-t_0}{\tau_r}}, \quad t_{2n-1} \le t < t_{2n}. \tag{43} $$

Note that the stress at the n-th injection and purge processes in Eqs. (42) and (43) can also be simplified when the duration time of injection and purge are fixed at T. From Eqs. (42) and (43), the stresses can be modified as

$$ {}^{\text{inj.}}\sigma_n(t) = -\sigma_{\text{sat.}} + \sigma_{\text{sat.}}\alpha \cdot e^{-\frac{t-t_0}{\tau_s}} \sum_{i=0}^{2(n-1)} \left(-e^{\frac{T}{\tau_s}}\right)^i + \sigma_{\text{sat.}}(1-\alpha) \cdot e^{-\frac{t-t_0}{\tau_r}} \sum_{i=0}^{2(n-1)} \left(-e^{\frac{T}{\tau_r}}\right)^i + \sigma_0 \cdot e^{-\frac{t-t_0}{\tau_r}} \tag{44a} $$

$$ = -\sigma_{\text{sat.}} + \sigma_{\text{sat.}}\alpha \cdot e^{-\frac{t-t_{2(n-1)}}{\tau_s}} \sum_{i=0}^{2(n-1)} \left(-e^{-\frac{T}{\tau_s}}\right)^i + \sigma_{\text{sat.}}(1-\alpha) \cdot e^{-\frac{t-t_{2(n-1)}}{\tau_r}} \sum_{i=0}^{2(n-1)} \left(-e^{-\frac{T}{\tau_r}}\right)^i + \sigma_0 \cdot e^{-\frac{t-t_0}{\tau_r}}, \; t_{2(n-1)} \le t < t_{2n-1}, \tag{44b} $$

$$ {}^{\text{purg.}}\sigma_n(t) = \sigma_{\text{sat.}}\alpha \cdot e^{-\frac{t-t_0}{\tau_s}} \sum_{i=0}^{2n-1} \left(-e^{\frac{T}{\tau_s}}\right)^i + \sigma_{\text{sat.}}(1-\alpha) \cdot e^{-\frac{t-t_0}{\tau_r}} \sum_{i=0}^{2n-1} \left(-e^{\frac{T}{\tau_r}}\right)^i + \sigma_0 \cdot e^{-\frac{t-t_0}{\tau_r}} \tag{45a} $$

$$ = -\sigma_{\text{sat.}}\alpha \cdot e^{-\frac{t-t_{2n-1}}{\tau_s}} \sum_{i=0}^{2n-1} \left(-e^{-\frac{T}{\tau_s}}\right)^i - \sigma_{\text{sat.}}(1-\alpha) \cdot e^{-\frac{t-t_{2n-1}}{\tau_r}} \sum_{i=0}^{2n-1} \left(-e^{-\frac{T}{\tau_r}}\right)^i + \sigma_0 \cdot e^{-\frac{t-t_0}{\tau_r}}, \; t_{2n-1} \le t < t_{2n}. \tag{45b} $$

In Eqs. (44) and (45), the analytical solutions clearly express the stress in terms of the elastic properties and relaxation properties in different forms with the viscoelastic relation in Eq. (21). The models given in Eqs. (44) and (45) are assumed to be proportional to the concentration of analyte in the gas phase C_g, and $\sigma_{sat.}$ is related to the amplitude of the signal. Similarly, with the analytical solutions of the elastic models in Eqs. (34b) and (35b), the terms t_{2n-1} and $t_{2(n-1)}$ in Eqs. (44b) and (45b) denote the time when the signal starts to rise and to decay for the corresponding steps of the rectangular pulse wave-like injection-purge cycles, respectively. Again, since the signal output of the nanomechanical sensing is directly proportional to the concentration $C(t)$ as described in Sec. III A [Eq. (7)], the signal output is analytically derived for the rectangular multistep injection-purge cycles with viscoelastic materials. It should be noted that the analytical solutions assume the first-order kinetics to the single analyte as shown in Eq. (8). Thus, to describe a multicomponent system, such as complex mixtures, some additional assumptions or some other equations are required.

V. RESULTS AND DISCUSSION

A. Numerical calculations of nanomechanical sensing coated with viscoelastic material

In this section, the responses of viscoelastic material-coated nanomechanical sensing are numerically calculated using the

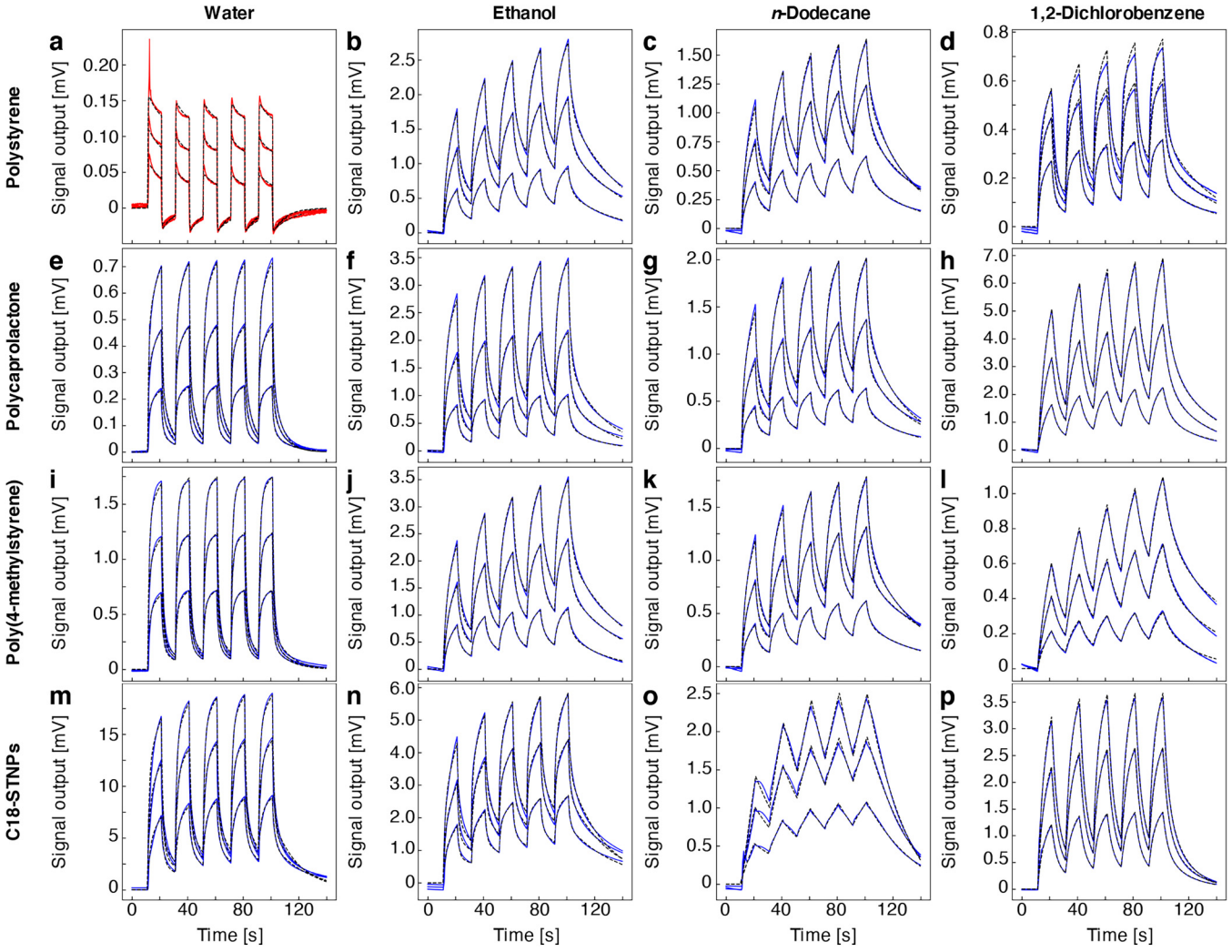

FIG. 7. Experimentally measured signal responses of viscoelastic material-coated MSS to four different analytes with different concentrations. The signal responses for polystyrene (a)–(d), polycaprolactone (e)–(h), poly(4-methylstyrene) (i)–(l), and alkyl-functionalized silica-titania hybrid nanoparticles (C_{18}-STNPs) (m–p) are shown. Red and blue lines are the original signal outputs and black dashed lines show the numerically calculated responses using Eqs. (44) and (45). The overshoot tendency in Eq. (46) is represented by red lines [observed only in (a)], and the conditions with no overshoot tendency are denoted by blue lines. The exposed gases used in this study are water [(a), (e), (i), and (m)], ethanol [(b), (f), (j), and (n)], *n*-dodecane [(c), (g), (k), and (o)], and 1,2-dichlorobenzene [(d), (h), (i), and (p)]. The concentration is varied with 10%, 20%, and 30% of the saturated vapors.

TABLE I. The optimized parameters for each VOC/polymer combination.

Receptor	VOC	C_g^a (%)	$\gamma \cdot \sigma_{sat.}$ (mV)	τ_s (s)	τ_r (s)	E_U/E_R	Receptor	VOC	C_g^a (%)	$\gamma \cdot \sigma_{sat.}$ (mV)	τ_s (s)	τ_r (s)	E_U/E_R
PCL	Water	10	0.28	11.03	0.94	7.18	P4MS	Water	10	0.82	11.49	1.14	6.43
		20	0.52	7.89	0.70	6.90			20	1.36	10.04	0.97	7.26
		30	0.78	6.96	0.67	6.38			30	1.90	11.14	0.98	8.47
	Ethanol	10	1.29	23.82	1.72	6.47		Ethanol	10	1.60	26.92	2.25	4.11
		20	2.85	26.13	1.68	6.98			20	3.74	39.27	2.33	4.97
		30	4.56	25.28	1.60	7.00			30	5.48	38.96	2.26	5.12
	n-dodecane	10	0.95	31.21	1.65	5.49		*n*-dodecane	10	0.99	40.23	2.47	4.56
		20	2.06	32.19	1.58	5.74			20	2.23	47.42	2.36	5.01
		30	2.93	26.54	1.47	5.51			30	2.75	35.41	2.22	4.71
	ODCB[b]	10	3.27	30.28	4.16	3.18		ODCB[b]	10	0.50	26.85	4.88	1.96
		20	6.60	31.27	4.43	3.25			20	1.25	45.85	5.95	2.48
		30	10.16	33.30	4.68	3.36			30	2.11	60.60	6.83	2.71
PS	Water	10	0.01	15.92	0.21	348.46	C_{18}-STNPs	Water	10	12.00	24.50	1.62	6.28
		20	0.06	10.95	0.15	124.51			20	18.11	20.82	1.41	7.50
		30	0.11	8.91	0.18	69.35			30	22.84	17.74	1.06	9.11
	Ethanol	10	1.43	33.97	2.22	4.51		Ethanol	10	4.17	34.68	1.20	7.41
		20	3.18	42.61	2.25	4.87			20	6.53	29.55	1.18	7.10
		30	4.40	39.06	2.18	4.77			30	8.28	25.38	1.22	6.66
	n-dodecane	10	1.00	36.95	2.93	3.42		*n*-dodecane	10	1.37	61.93	61.95	2.71
		20	2.07	40.67	2.64	3.64			20	2.40	57.37	57.38	2.75
		30	2.55	30.02	1.96	3.63			30	3.30	48.95	48.96	2.45
	ODCB[b]	10	0.50	32.58	1.98	6.76		ODCB[b]	10	1.88	18.23	3.36	2.88
		20	0.86	34.35	1.99	6.90			20	3.39	16.46	3.39	2.72
		30	1.10	32.16	2.04	6.09			30	4.64	14.34	3.12	2.51

[a]Concentration of VOCs at the injection process [see also Eq. (26)]. Values correspond to P_a/P_o, where P_a and P_o denote the partial pressure and saturated vapor pressure, respectively.
[b]1,2-dichlrorobenzene.

models derived in Sec. IV B. As presented in Fig. 5, the signal output of elastic material-coated nanomechanical sensors only depends on the desorption time constant τ_s. When the desorption of the analyte is slow (e.g., $\tau_s = 120$ [s]), the analytes adsorbed and diffused into the coating film during the injection process do not completely desorb during the purge process, resulting in an increase in the baseline. In contrast, if the desorption time constant is fast enough such that the signal reaches a steady-state or an equilibrium state within the injection and purge processes, the signal obtains a symmetric response. Therefore, no baseline increase is observed.

When a viscoelastic material is used for a receptor layer of a nanomechanical sensor, the corresponding signal drastically changes. In the case of a single rectangular injection model with viscoelastic coating, Wenzel *et al.* widely discussed the detailed tendencies of signal responses.[15] For example, if sorption occurs faster than the relaxation process (i.e., $\tau_s \ll \tau_r$), the response derived from absorption-induced deformation yields higher signal output than the level of amplitude $\sigma_{sat.}$ because of a built-up of unrelaxed stress, followed by a decrease due to relaxation. Then, the signal response exhibits an overshoot, depicted as red signals in Fig. 6, with long enough duration (dashed lines). Wenzel *et al.* derived the condition for which the response exhibits an overshoot as

$$\frac{E_U}{E_R} - \frac{\tau_s}{\tau_r} > 0, \tag{46}$$

only if $E_U > E_R$ with long duration.

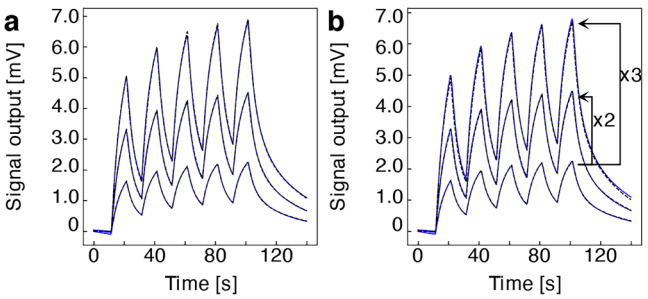

FIG. 8. Experimentally measured signal responses of PCL-coated MSS to 1,2-dichlorobenzene. (a) Result of Fig. 7(h). (b) Fitting curves with optimized parameters calculated from 10% signal response. Corresponding $\gamma \cdot \sigma_{sat.}$ is multiplied by 20%/10% and 30%/10%, respectively.

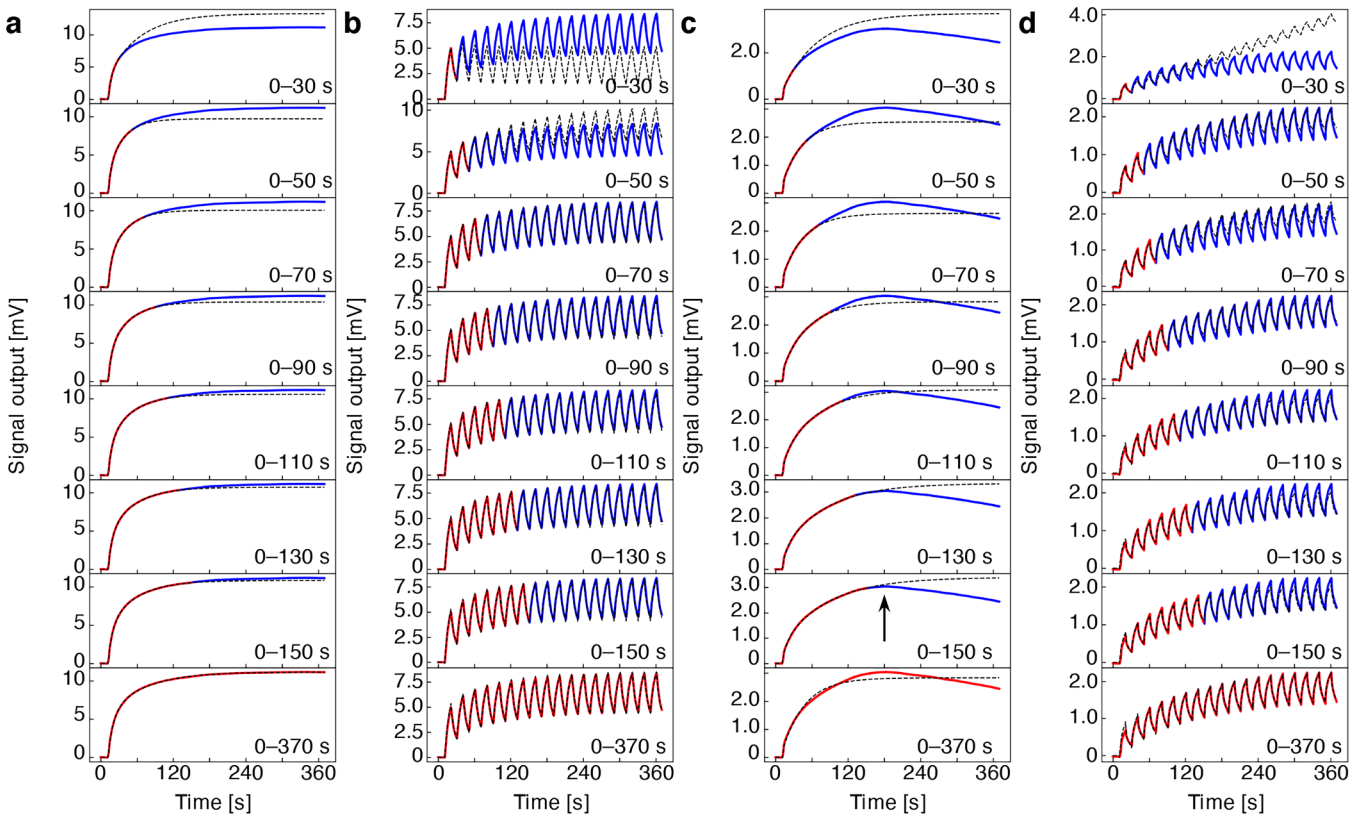

FIG. 9. Fitting accuracy between a single injection signal response and multistep injection-purge cycle. (a) and (b) 1,2-Dichlorobenzene/PCL and (c) and (d) *n*-dodecane/PS are shown ($P_a/P_o = 30\%$). Red colored signal responses are used for optimizing each fitting curve. Black dashed lines are the corresponding fitting curves. Black arrow indicates the point where the secondary or tertiary viscoelastic response may start taking place.

If the duration is shorter than the time $t_{max.}$ when the relaxation starts to decay (i.e., $T \leq t_{max.}$), it is expected that the signal does not yield the overshoot characteristics (Fig. 6). Importantly, the baseline at time t_{2n}, when the injection starts, exhibits a clear correlation with the signal responses of long duration (dotted lines). These characteristic baseline transitions clearly indicate the viscoelastic response by a sorption-induced nanomechanical sensing. If the desorption time constant is small, the overshoot can be observed even in the short duration (10 s). In such a case, the baseline monotonously decreases and reaches the steady-state. Conversely, when the desorption time constant is relatively large, the baseline shows an overshoot-like tendency, i.e., the baseline first increases, then decreases after $t_{max.}$ (Fig. 6; see also Figs. S1 and S2 in the supplementary material). In the case that the condition given in Eq. (46) does not hold, the overshoot does not occur as shown in blue lines in Fig. 6.

The nanomechanical sensing responses with different durations of injection-purge cycles are also numerically simulated using the model derived in Sec. IV B as described in the Appendix. Using Eqs. (42) and (43), it is possible to design the effective injection-purge sequence depending on the target features to be extracted.

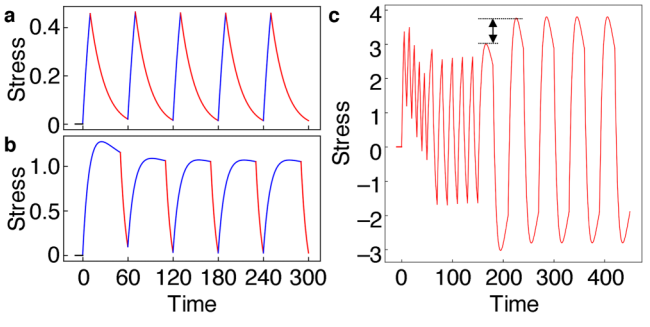

FIG. 10. Dynamic stress change derived from sorption-induced deformation estimated by Eqs. (42) and (43) with different durations. (a) The injection and purge durations are set at 10 and 50 s, respectively. $E_U/E_R = 1.75$; $\tau_r = 25$ [s]; $\tau_s = 30$ [s]; $\sigma_{sat.} = 1$; and $t_0 = 0$. (b) The injection and purge durations are set at 50 and 10 s, respectively. $E_U/E_R = 1.75$; $\tau_r = 25$ [s]; $\tau_s = 10$ [s]; $\sigma_{sat.} = 1$; $t_0 = 0$. Blue and red lines indicate the injection and purge responses, respectively. (c) The numbers of injection-purge cycles are 15 with different durations T; 1–5 cycles, 5 s; 6–10 cycles, 10 s; and 11–15 cycles, 30 [s]. $E_U/E_R = 10$; $\tau_r = 15$ [s]; $\tau_s = 10$ [s]; $\sigma_{sat.} = 1$; and $t_0 = 0$.

B. Estimation of parameters

The experimentally obtained signal output of MSS was fitted using Eqs. (44) and (45) and the parameters are optimized. We fabricated viscoelastic material-coated MSS with three different viscoelastic polymers, PS, PCL, and P4MS, which are a series of hydrophobic polymers. We also fabricated viscoelastic alkyl-functionalized inorganic nanoparticles, i.e., octadecyl-functionalized silica-titania hybrid nanoparticles (C_{18}-STNPs).[9,22] Their signal responses to a varieties of volatile organic compounds (VOCs), i.e., ethanol, *n*-dodecane, and 1,2-dichlorobenzene, as well as water were measured.

Since the signal output is directly proportional to the concentration of an analyte in a coating film as described in Sec. III A, the signal output of MSS V_{out} can be given by

$$V_{\text{out}}(t) = \gamma \cdot C(t) + V_{\text{out}}(t_0) \tag{47a}$$

for the elastic model, and

$$V_{\text{out}}(t) = \gamma \cdot \sigma(t) + V_{\text{out}}(t_0) \tag{47b}$$

for the viscoelastic model, where γ and $V_{\text{out}}(t_0)$ are the proportionality factor and the signal output at $t = t_0$ (i.e., baseline), respectively. When $\gamma = 1$, the analytical models in Eqs. (34)–(35) and (42)–(43) are directly applicable to the sensing signal of MSS. We fit the signal output with Eqs. (44) and (45) for five cycles. The parameters are optimized through non-linear least squares curve fitting using Python with SciPy module. The details are presented in Sec. II.

Figures 7(a)–7(h) show the fitting results for the signal outputs of viscoelastic polymer-coated MSS. The optimized parameters are summarized in Table I. The signal responses are well fitted with the derived equations for five injection-purge cycles. The optimized stress relaxation parameters (E_U/E_R and τ_r) of each analyte/polymer pair show a good agreement in the different concentrations, except water/PS pair. In the case of the signal response of PS-coated MSS to water vapor, the strong overshoot was observed. According to the result in Fig. 6, the tendency of a strong overshoot indicates that the diffusion time constant τ_s is significantly larger than the relaxation time constant τ_r ($\tau_s \ll 0.1$). It is probably because the diffusion speed is extremely slow, due to the hydrophobic nature of PS, and the signal response only reflects the adsorption process, which is generally much faster than the absorption process.[13] Such an extremely small time constant cannot be numerically calculated (i.e., $e^{-1000} \rightarrow e^{-\infty} = 0$), resulting in the unoptimized parameters. Importantly, each baseline transition clearly fits with the results in the numerical solutions (Fig. 6). Water/PS shows the overshoot response; therefore, the baseline rapidly decreases, while the other cases do not exhibit overshoot tendency with relatively large τ_s, leading to the increase in the baseline.

We also demonstrated the fitting with alkyl-functionalized inorganic nanoparticles [Figs. 7(i)–7(l)]. Generally, inorganic bulk materials tend to have elastic properties, while the nanoparticles functionalized with organic groups often exhibit viscoelastic behavior. The signal responses of C_{18}-STNPs are well fitted with the derived equations for viscoelastic material in Eqs. (44) and (45); however, they do not fit well with the elastic equations in Eqs. (34) and (35) (data not shown). This result clearly indicates that the alkyl-functionalized nanoparticles also exhibit the viscoelastic behavior.

It should be noted that most of the analyte/coating pairs show the amplitude parameter $\gamma \cdot \sigma_{\text{sat.}}$ proportional to the concentrations of analytes. As shown in Fig. 8, the signal responses of different concentrations (20% and 30%) can be entirely predicted with the fitting parameters extracted from the 10% signal response by simply multiplying the amplitude parameter $\gamma \cdot \sigma_{\text{sat.}}$. The good agreement of the concentration dependency demonstrates that the predictive capabilities of the theoretical models.

Importantly, the optimized parameters generally depend on the least squares techniques and the initial fitting parameters (see also Fig. S3 and Table S1). When the measured signal responses are short (e.g., 30 s), then the parameters extracted from the experimental results cannot predict the entire signal responses (Fig. 9; see also Fig. S4 for the coefficient of determination, R^2). If the signal response seems not to reach the steady state, the parameters extracted from a single injection procedure do not fit well to the experimental results (i.e., 1,2-dichlorobenzene/PCL) [Fig. 9(a); Fig. S4a]. Conversely, in the case of the multistep injection-purge cycle, the curves predicted by the extracted parameters fit well with the experimental results [Fig. 9(b); Fig. S4b]. Furthermore, polymers sometimes exhibit the secondary and tertiary viscoelastic relaxation properties.[17] As can be seen in Fig. 9(d), PS changes the signal response at approximately 180 s, followed by a decrease in the signal output. In such cases, it is difficult to measure the response of the steady state, thereby resulting in the extraction of less accurate parameters. Conversely, in the case of the multistep injection-purge cycles, the analyte desorbs from a receptor during the purge step, thereby minimizing such changes in the elastic property [Fig. 9(d); Fig. S4d]. Therefore, the optimized parameters extracted from a couple of injection-purge cycles can be clearly predicted by the experimental responses.

VI. CONCLUSION

The theory of the nanomechanical sensors coated with a viscoelastic material proposed by Wenzel *et al.*[15] was extended to the multistep injection-purge cycle model. This theory includes the stress relaxation effects of a viscoelastic coating film and represents the accurate signal responses. The numerical calculations show very good agreement with the trends observed in the experimental results measured by MSS coated with different viscoelastic materials, including polymers and inorganic nanoparticles. Therefore, the theoretical model can be utilized to extract values of the various coating parameters as well as the coating film/analyte parameters. More importantly, the present derived model can be used to predict and/or analyze the signal responses of a nanomechanical sensor during the absorption and desorption processes without measuring until the signal reaches the steady-state. By measuring a couple of injection-purge cycles with relatively short duration, the actual values of the coating properties can be extracted.

Analysis of the transient response using the presented models will be beneficial for the improvement in recognition accuracy of analytes based on scientific interpretation. The optimized parameters can be extracted from the multistep injection-purge cycles more accurately than that extracted from a single injection or purge curve and, hence, the optimized parameters (e.g., τ_s) can be directly used as an effective index for the identification of gas species as proposed in the previous literature.[16] The presented model can be utilized for the analyses of repeated injection-purge cycles with a short duration, contributing to the development of the practical artificial olfaction.

SUPPLEMENTARY MATERIAL

See the supplementary material for the detailed numerical calculations of viscoelastic responses.

ACKNOWLEDGMENTS

We thank Mr. Takahiro Nemoto, Center for Functional Sensor & Actuator (CFSC), National Institute for Materials Science (NIMS), Japan for fruitful discussion on this present study. K.M. acknowledges the International Center for Young Scientists (ICYS) program, NIMS. This study was financially supported by JST CREST (No. JPMJCR1665); a Grant-in-Aid for Scientific Research (A), MEXT, Japan (No. 18H04168); Grant-in-Aid for Challenging Research (Pioneering) (No. 20K20554); the Public/Private R&D Investment Strategic Expansion Program (PRISM), Cabinet Office, Japan; the Izumi Science and Technology Foundation (No. 2020-J-070); ICYS, NIMS; CFSN, NIMS; and the World Premier International Research Center Initiative (WPI) on Materials Nanoarchitectonics (MANA), NIMS.

APPENDIX: PREDICTION OF INJECTION-PURGE CYCLES WITH DIFFERENT DURATION

The viscoelastic model derived in Sec. IV B can be utilized for predicting and simulating the signal response of injection-purge cycles with different durations. For example, in the case of following parameters: $E_U/E_R = 1.75$; $\tau_r = 25$ [s]; $\tau_s = 10$ [s], the signal response yields significant baseline drift (see Fig. 6), while each of injection and purge set at 10 and 50 s yields the signal responses without baseline drift [Fig. 10(a)]. Similarly, the small diffusion time constant $\tau_s = 10$ [s] shows a negative baseline shift due to the viscoelastic behavior, while the baseline drifts can be minimized by tuning each duration time of the injection and purge as 50 and 10 s, respectively [Fig. 10(b)]. Additionally, when we change the duration time, for example, from 10 s to 30 s, the first and second injections yield the different intensities [Fig. 10(c), black arrow]. After optimizing the parameters from the experimental results, it is possible to predict and simulate the signal responses with any kind of injection-purge sequence using the presented model.

DATA AVAILABILITY

The data that support the findings of this study are available from the corresponding author upon reasonable request.

REFERENCES

[1]J. K. Gimzewski, Ch. Gerber, E. Meyer, and R. R. Schlittler, "Observation of a chemical-reaction using a micromechanical sensor," Chem. Phys. Lett. **217**, 589–594 (1994).
[2]K. M. Goeders, J. S. Colton, and L. A. Bottomley, "Microcantilevers: Sensing chemical interactions via mechanical motion," Chem. Rev. **108**, 522–542 (2008).
[3]G. Yoshikawa, T. Akiyama, S. Gautsch, P. Vettiger, and H. Rohrer, "Nanomechanical membrane-type surface stress sensor," Nano Lett. **11**, 1044–1048 (2011).
[4]K. Minami, K. Shiba, and G. Yoshikawa, "Discrimination of structurally similar odorous molecules with various concentrations by using a nanomechanical sensor," Anal. Methods **10**, 3720–3726 (2018).
[5]K. Minami, G. Imamura, T. Nemoto, K. Shiba, and G. Yoshikawa, "Pattern recognition of solid materials by multiple probe gases," Mater. Horiz. **6**, 580–586 (2019).
[6]H. H.-M. Yeung, G. Yoshikawa, K. Minami, and K. Shiba, "Strain-based chemical sensing using metal-organic framework nanoparticles," J. Mater. Chem. A **8**, 18007–18014 (2020).
[7]T. Yakabe, G. Imamura, G. Yoshikawa, M. Kitajima, and A. N. Itakura, "Hydrogen detection using membrane-type surface stress sensor," J. Phys. Commun. **4**, 025005 (2020).
[8]G. Imamura, K. Shiba, and G. Yoshikawa, "Smell identification of spices using nanomechanical membrane-type surface stress sensors," Jpn. J. Appl. Phys. **55**, 1102b3 (2016).
[9]K. Shiba, R. Tamura, G. Imamura, and G. Yoshikawa, "Data-driven nanomechanical sensing: Specific information extraction from a complex system," Sci. Rep. **7**, 3661 (2017).
[10]K. Shiba, R. Tamura, T. Sugiyama, Y. Kameyama, K. Koda, E. Sakon, K. Minami, H. T. Ngo, G. Imamura, K. Tsuda, and G. Yoshikawa, "Functional nanoparticles-coated nanomechanical sensor arrays for machine learning-based quantitative odor analysis," ACS Sens. **3**, 1592–1600 (2018).
[11]M. Nishikawa, T. Murata, S. Ishihara, K. Shiba, L. K. Shrestha, G. Yoshikawa, K. Minami, and K. Ariga, "Discrimination of methanol from ethanol in gasoline using membrane-type surface stress sensor coated with copper(I) complex," Bull. Chem. Soc. Jpn. **94**, 2 (2020).
[12]J. Yan, X. Guo, S. Duan, P. Jia, L. Wang, C. Peng, and S. Zhang, "Electronic nose feature extraction methods: A review," Sensors **15**, 27804–31 (2015).
[13]Z. Y. Hu, T. Thundat, and R. J. Warmack, "Investigation of adsorption and absorption-induced stresses using microcantilever sensors," J. Appl. Phys. **90**, 427–431 (2001).
[14]D. W. Dareing and T. Thundat, "Simulation of adsorption-induced stress of a microcantilever sensor," J. Appl. Phys. **97**, 043526 (2005).
[15]M. J. Wenzel, F. Josse, S. M. Heinrich, E. Yaz, and P. G. Datskos, "Sorption-induced static bending of microcantilevers coated with viscoelastic material," J. Appl. Phys. **103**, 064913 (2008).
[16]G. Imamura, K. Shiba, G. Yoshikawa, and T. Washio, "Analysis of nanomechanical sensing signals; physical parameter estimation for gas identification," AIP Adv. **8**, 075007 (2018).
[17]V. N. Pokrovskii, *The Mesoscopic Theory of Polymer Dynamics*, 2nd ed. (Springer, New York, 1975).
[18]N. G. Hockstein, E. R. Thaler, D. Torigian, W. T. Miller Jr., O. Deffenderfer, and C. W. Hanson, "Diagnosis of pneumonia with an electronic nose: Correlation of vapor signature with chest computed tomography scan findings," Laryngoscope **114**, 1701–1075 (2004).
[19]A. Zakaria, A. Y. M. Shakaff, M. J. Masnan, F. S. A. Saad, A. H. Adom, M. N. Ahmad, M. N. Jaafar, A. H. Abdullah, and L. M. Kamarudin, "Improved maturity and ripeness classifications of *Magnifera Indica* cv. Harumanis mangoes through sensor fusion of an electronic nose and acoustic sensor," Sensors **12**, 6023–6048 (2012).
[20]H. P. Lang, F. Loizeau, A. Hiou-Feige, J. P. Rivals, P. Romero, T. Akiyama, C. Gerber, and E. Meyer, "Piezoresistive membrane surface stress sensors for

characterization of breath samples of head and neck cancer patients," Sensors **16**, 1149 (2016).
[21]G. Yoshikawa, T. Akiyama, F. Loizeau, K. Shiba, S. Gautsch, T. Nakayama, P. Vettiger, N. F. de Rooij, and M. Aono, "Two-dimensional array of piezoresistive nanomechanical membrane-type surface stress sensor (MSS) with improved sensitivity," Sensors **12**, 15873–15887 (2012).
[22]K. Shiba, T. Sugiyama, T. Takei, and G. Yoshikawa, "Controlled growth of silica-titania hybrid functional nanoparticles through a multistep microfluidic approach," Chem. Commun. **51**, 15854–15857 (2015).
[23]G. Yoshikawa, "Mechanical analysis and optimization of a microcantilever sensor coated with a solid receptor film," Appl. Phys. Lett. **98**, 173502 (2011).
[24]G. G. Stoney, "The tension of metallic films deposited by electrolysis," Proc. R. Soc. London Ser. A **82**, 172–175 (1909).
[25]W.-H. Chu, M. Mehregany, and R. L. Mullen, "Analysis of tip deflection and force of a bimetallic cantilever microactuator," J. Micromech. Microeng. **3**, 4–7 (1993).
[26]F. Loizeau, T. Akiyama, S. Gautsch, P. Vettiger, G. Yoshikawa, and N. F. de Rooij, "Comparing membrane- and cantilever-based surface stress sensors for reproducibility," Sens. Actuators A **228**, 9–15 (2015).
[27]G. Imamura, K. Shiba, and G. Yoshikawa, "Finite element analysis on nanomechanical detection of small particles: Toward virus detection," Front. Microbiol. **7**, 488 (2016).
[28]K. Minami and G. Yoshikawa, "Finite element analysis of interface dependence on nanomechanical sensing," Sensors **20**, 1518 (2020).
[29]K. Minami and G. Yoshikawa, "Effects of partial attachment at the interface between receptor and substrate on nanomechanical cantilever sensing," Sens. Actuator A **319**, 112533 (2021).
[30]J. D. Ferry, *Viscoelastic Properties of Polymers*, 3rd ed. (Wiley, New York, 1980), p. 608.
[31]W. Flugge, *Viscoelasticity*, 2nd ed. (Springer, New York, 1975).
[32]G. Yoshikawa, H. P. Lang, T. Akiyama, L. Aeschimann, U. Staufer, P. Vettiger, M. Aono, T. Sakurai, and C. Gerber, "Sub-ppm detection of vapors using piezoresistive microcantilever array sensors," Nanotechnology **20**, 015501 (2009).